

# Kinetic and Thermodynamic Characterization of Dihydrotestosterone-Induced Conformational Perturbations in Androgen Receptor Ligand-Binding Domain

Ravi Jasuja, Jagadish Ulloor, Christopher M. Yengo, Karen Choong, Andrei Y. Istomin, Dennis R. Livesay, Donald J. Jacobs, Ronald S. Swerdloff, Jaroslava Mikšovská, Randy W. Larsen, and Shalender Bhasin

Section of Endocrinology, Diabetes, and Nutrition (R.J., J.U., K.C., S.B.), Boston University School of Medicine, Boston, Massachusetts 02199; Division of Endocrinology (R.J.), Charles R. Drew University of Medicine and Science, Los Angeles, California 90059; Departments of Biology (C.M.Y.), Physics and Optical Sciences (A.Y.I., D.J.J.), and Computer Science (A.Y.I., D.R.L.) and Bioinformatics Research Center (A.Y.I., D.R.L.), University of North Carolina, Charlotte, North Carolina 28223; Division of Endocrinology (R.S.S.), Harbor-UCLA Medical Center, Los Angeles Biomedical Research Institute, Torrance, California 90502; Department of Chemistry and Biochemistry (J.M.), Florida International University, Miami, Florida 33181; and Department of Chemistry (R.W.L.), University of South Florida, Tampa, Florida 33620

Ligand-induced conformational perturbations in androgen receptor (AR) are important in coactivator recruitment and transactivation. However, molecular rearrangements in AR ligand-binding domain (AR-LBD) associated with agonist binding and their kinetic and thermodynamic parameters are poorly understood. We used steady-state second-derivative absorption and emission spectroscopy, pressure and temperature perturbations, and 4,4'-bis-anilinothalene 8-sulfonate (bis-ANS) partitioning to determine the kinetics and thermodynamics of the conformational changes in AR-LBD after dihydrotestosterone (DHT) binding. In presence of DHT, the second-derivative absorption spectrum showed a red shift and a change in peak-to-peak distance. Emission intensity increased upon DHT binding, and center of spectral mass was blue shifted, denoting conformational changes resulting in more hydrophobic environment for tyrosines and tryptophans within a more compact DHT-bound receptor. In pressure perturbation calorimetry, DHT-induced energetic stabilization increased the Gibbs free energy of unfolding to  $8.4 \pm 1.3$  kcal/mol from  $3.5 \pm 1.6$  kcal/mol. Bis-ANS partitioning studies revealed that upon DHT binding, AR-LBD underwent biphasic rearrangement with a high activation energy (13.4 kcal/mol). An initial, molten globule-like burst phase ( $k \sim 30 \text{ sec}^{-1}$ ) with greater solvent accessibility was followed by rearrangement ( $k \sim 0.01 \text{ sec}^{-1}$ ), leading to a more compact conformation than apo-AR-LBD. Molecular simulations demonstrated unique sensitivity of tyrosine and tryptophan residues during pressure unfolding with rearrangement of residues in the coactivator recruitment surfaces distant from the ligand-binding pocket. In conclusion, DHT binding leads to energetic stabilization of AR-LBD domain and substantial rearrangement of residues distant from the ligand-binding pocket. DHT binding to AR-LBD involves biphasic receptor rearrangement including population of a molten globule-like intermediate state. (*Molecular Endocrinology* 23: 1231–1241, 2009)

ISSN Print 0888-8809 ISSN Online 1944-9917

Printed in U.S.A.

Copyright © 2009 by The Endocrine Society

doi: 10.1210/me.2008-0304 Received August 25, 2008. Accepted May 7, 2009.

First Published Online May 14, 2009

Abbreviations: AR, Androgen receptor; ASA, solvent-accessible surface area; bis-ANS, 4,4'-bis-anilinothalene 8-sulfonate; CM, center of spectral mass; CoaBC, coactivator binding cleft; CoaRS1, coactivator recruitment surface 1; DHT, dihydrotestosterone; DTT, dithiothreitol; FA, fluorescent analog; GnHCl, guanidinium hydrochloride; GST, glutathione S-transferase; LBD, ligand-binding domain; LBI, ligand-binding interface; mP, millipolarization units; RMSD, root mean square deviation; SARMS, selective androgen receptor modulator.

Androgen receptor (AR) activation plays important roles in diverse physiological responses ranging from male sexual maturation to skeletal muscle growth (1–6). The binding of androgens to the ligand-binding domain (LBD) of the AR (AR-LBD) initiates a signaling cascade that results in nuclear translocation of the liganded receptor and transcriptional modulation of target genes (7–11).

Members of the nuclear hormone receptor family of proteins, including AR, possess distinct domains for ligand binding, DNA binding, and transactivation. AR-LBD shows well conserved homology with the progesterin, glucocorticoid, and mineralocorticoid receptors. The x-ray crystal structure of domains of several nuclear receptor proteins, including estrogen receptor  $\alpha$  and  $\beta$ , progesterone receptor, and retinoic acid receptors, has been published (12–14). The domains of these receptors have striking structural similarities even with low sequence homology.

Androgen receptor is a 919-amino acid protein (110 kDa) with a transactivation domain spanning 1–514, a DNA-binding domain from 545–675, and the LBD from 690–919 amino acids (15–18). Ligand-mediated transcriptional modulation can be regulated at several steps. Initial discrimination among ligands is exercised at the ligand recognition step that is affected mostly by the hydrophobic residues and their interaction with the steroidal ring structure. Upon ligand binding, heat-shock proteins dissociate from the receptor and the residue surfaces in the transactivation function sequence AF2 within the AR-LBD (19–22) are exposed. Coregulator proteins associate with the AF2 region and promote the nuclear translocation of the complex (23–31). A common consensus LXXLL motif in the coregulators interacts with exposed surfaces in the AF2 region of AR-LBD (32, 33). Typically, the LBD contains up to 12 helices arranged in such a manner that upon ligand binding, helix 12 undergoes repositioning (34, 35).

Conformational states of a receptor can govern biological signaling by regulating ligand selectivity, protein recruitment for activation or suppression, and subsequent transcriptional amplification by modulating residence time on the DNA response elements (36). Therefore, an understanding of ligand-specific conformational changes is central to our efforts at rational design of selective ligands with discrete signaling properties. The crystal structure of AR-LBD complexed with a series of ligands have been published, but the crystal structure of the corresponding unliganded form is not known (37–39). Consequently, the dynamics of rearrangements that are associated with agonist binding are poorly understood and were the subject of this investigation. Homology modeling of AR with other members of the nuclear receptor family and proteolysis studies suggest that agonist binding leads to substantial reorganization of the receptor fragments (40–42), but the kinetic and thermodynamic parameters that govern these conformational changes have not been studied. We tested the hypothesis that receptor conformational state is highly flexible in the absence of ligand but achieves a well-defined, energetically stable form in the presence of ligand. We used a number of biophysical techniques, second-derivative absorption spectra, emission spectra, pressure perturbation calorimetry, temperature dependence, and 4, 4'-bis-anilino-naphthalene 8-sulfonate (bis-ANS)

partitioning, to determine their kinetics and thermodynamics of the dihydrotestosterone (DHT)-induced conformational perturbations in AR-LBD. In conjunction with the experimental data, we performed molecular dynamics simulations to show that DHT association results in substantial rearrangement in coregulator recruitment surfaces within AR-LBD, distant from the ligand-binding pocket.

## Results

### Second-derivative absorption

Tyrosine and tryptophan possess overlapping absorption bands in the UV region. The second derivative of absorption spectrum follows the Beer-Lambert law and suppresses effectively the broad, nonaromatic spectral contributions, thereby allowing the quantification of solvent perturbations in the microenvironment of tyrosine and tryptophan residues. Second-derivative absorption spectroscopy has been used widely to study conformational perturbations in proteins (42–47). The most generalized quantitative method, described by Ragone *et al.* (43), employs the ratio between two second-derivative peak to peak distances ( $\alpha/\beta$  ratio) to assess average solvent exposure of amino acid residues.

We obtained the second-derivative ( $d^2A/d\lambda^2$ ) spectra of AR-LBD in the absence and presence of DHT to identify the extent of ligand-induced conformational changes in the receptor domain. The second derivative spectrum of AR-LBD shows two maxima centered at 278 and 287 nm (Fig. 1, A and B). The peak to trough distance between maximum at 278 nm and the minimum at 273 nm is indicated as  $\alpha$ , and the peak to trough distance between the maximum at 287 nm and minimum at 282 nm is indicated as  $\beta$ . The solvent accessibility parameters specifically for the tyrosine residues were quantitated by the  $\alpha/\beta$  ratio. In the presence of DHT, the second-order derivative

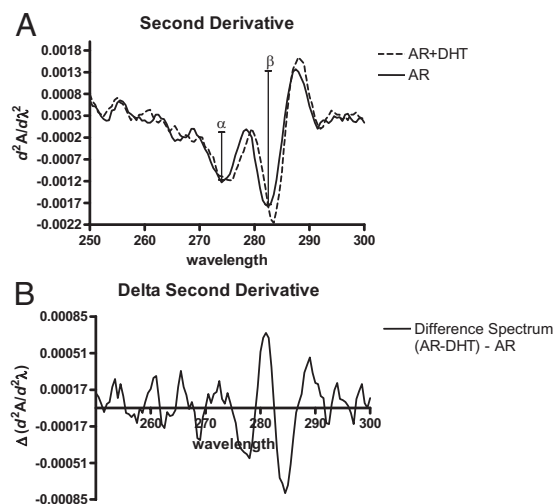


**FIG. 1.** Second-derivative absorption spectra of AR-LBD were derived in the absence and presence of DHT. A, Absolute absorption spectra; B, difference spectra in the UV region. The peak to trough distance between the maximum at 278 and the maximum at 273 nm is indicated as  $\alpha$ , and the peak to trough distance between the maximum at 287 and minimum at 282 nm is indicated as  $\beta$ .

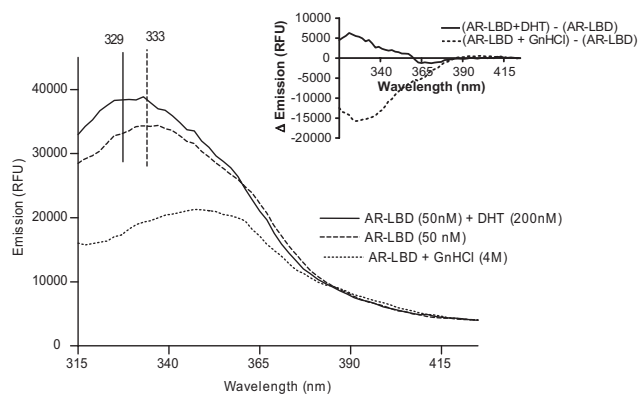


**FIG. 2.** Effect of DHT binding and GnHCl denaturation of AR-LBD on the emission spectra of intrinsic tyrosine and tryptophan residues. Fifty nanomolar AR-LBD (2 mM DTT in 50 mM Tris-HCl) was excited at 278 nm and data were collected from 300–450 nm through a 1-nm slit. *Inset*, Difference spectra after addition of DHT (*solid line*) or 4 M GnHCl (*dashed line*) to elucidate the changes in emission peak and intensity of AR-LBD.

spectrum displayed a red shift, suggesting DHT-induced change in the environment of some of the tyrosine and/or tryptophan residues. Also, in presence of DHT, the  $\alpha/\beta$  ratio decreased from 0.42–0.34, suggesting an increase in hydrophobic environment of tyrosine residues within a more compact DHT-bound receptor.

### Effect of DHT and guanidinium hydrochloride on tryptophan and tyrosine emission

Intrinsic tyrosine and tryptophan residues are distributed along the helices in AR-LBD and provide a sensitive tool to identify conformational rearrangements in AR-LBD. Integrated emission intensity, center of spectral mass (CM), and the excited state lifetimes change significantly in response to subtle changes in the microenvironment of residues. Emission spectra of free and DHT-bound AR-LBD are presented in Fig. 2. In the presence of DHT, emission intensity increased slightly and CM was blue shifted, denoting increased hydrophobicity in the vicinity of tryptophan and tyrosine residues. Similar results were obtained when the protein was excited at 295 nm instead of 278 nm to monitor tryptophan residues (not shown). Figure 2, *inset*, displays the difference spectra and highlights the diametrically opposite changes in emission profile upon addition of either guanidinium hydrochloride (GnHCl) or DHT. GnHCl-induced unfolding leads to a red shift in the center of mass of emission spectrum and a concomitant reduction in emission intensity. Collectively, these data suggest that ligand binding resulted in overall compactness in AR-LBD.

### Characterization of ligand-bound AR-LBD

To determine whether there are multiple equilibria of AR-LBD in the presence of the fluorescent analog (FA), we measured the fluorescence anisotropy of FA in the presence and absence of AR-LBD at varying viscosities at 10, 20, and 30 °C. Fig. 3 depicts the effect of viscosity on the steady-state anisotropy of the bound and free fluorescent analog. The data were fit to the Perrin equation (equation 1) to obtain the rotational correlation times of FA, free in solution (0.8 nsec) and bound to AR-LBD (19 nsec) (equation 2). The calculated and experimental values

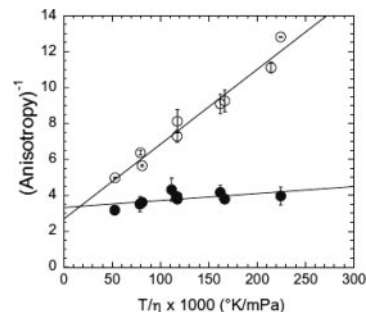


**FIG. 3.** Perrin plots of fluorescein-labeled testosterone (FA) bound to AR-LBD and free FA in solution. The steady-state anisotropy of 4 or 8 nM FA in the absence (○) and presence (●) of 50 nM LBD was obtained at different glycerol concentrations [to vary the viscosity ( $\eta$ )] at 20, 30, and 40 °C.

of the rotational correlation times agree closely for the free and bound species in the monomeric forms. In addition, we observed a linear dependence of  $1/\text{anisotropy}$  on the  $T/\eta$ , which indicates that only one species is getting depolarized, further supporting the notion that there is no detectable heterogeneity in binding modes of fluorescent androgen (FA) to the receptor protein. In an independent fluorescence correlation spectroscopy measurement, consistent with the steady-state anisotropy, we did not observe any aggregates from the plots of counts per second against acquisition time (data not shown).

### Pressure unfolding of AR-LBD

Tryptophan and tyrosine fluorescence was measured using excitation at either 278 or 295 nm and emission was scanned from 300–450 nm or 315–450 nm, respectively. Before pressure unfolding, AR-LBD with or without DHT was allowed to equilibrate in the pressure cell for 30 min in 50 mM Tris (pH 7.5). Figure 4 shows emission scans with 278 nm excitation. At ambient pressure, the maxima of emission wavelength of the protein for tyrosines and tryptophans were 320 nm ( $\lambda_{\text{ex}}$  278 nm) and 330 nm ( $\lambda_{\text{ex}}$  295 nm), respectively, indicating that the average environment of these residues is fairly hydrophobic. With progressive increase in pressure, the center of mass for the emission spectra red shifted, which is typical of the movement of aromatic residues into an aqueous environment. Similar effects on the emission spectra were observed when the samples were excited at either 295 or 278 nm, suggesting global unfolding of the protein. These data indicate that the tyrosine and tryptophan residues are gradually exposed to solvent as pressure is increased. The decrease in fluorescence intensity with a concomitant red shift in CM upon unfolding indicates that the pressure-unfolded state corresponds to an unfolding intermediate. We observed almost complete recovery of the integrated intensity with decompression, although some hysteresis was observed. We posit that during decompression, the conformational states that are populated may be energetically equivalent but conformationally distinct. During these pressure titrations, we did not observe any turbidity or significant loss of integrated intensity that may denote precipitation.

At 25 °C, the Gibbs free energy ( $\Delta G_u$ ) and volume change ( $\Delta V_u$ ) for AR-LBD were found to be  $3.5 \pm 0.3$  kcal/mol and  $33.8 \pm 1.6$  ml/mol in the absence of DHT and  $8.4 \pm 0.7$  kcal/mol and  $65.7 \pm 2.1$  ml/mol, respectively, in the presence of DHT

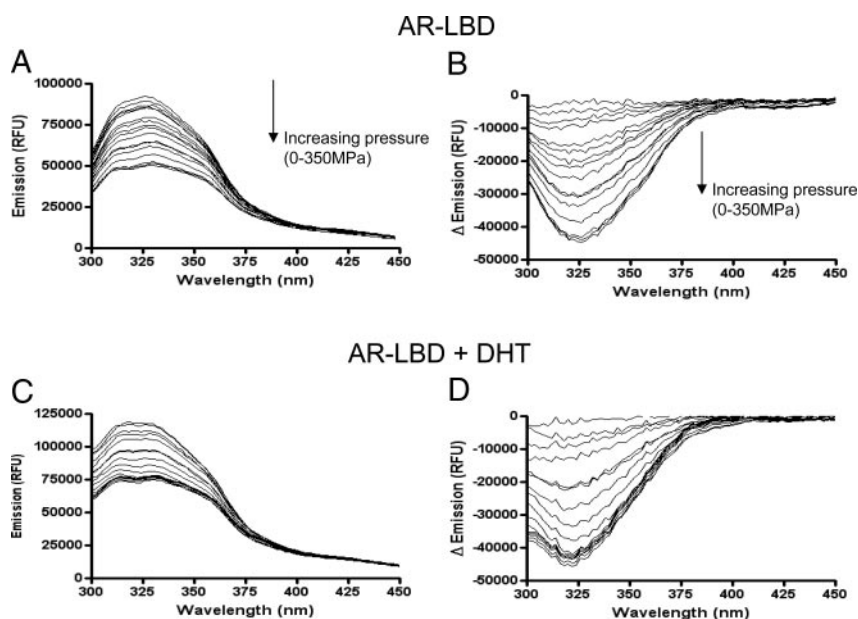


**FIG. 4.** Pressure-induced denaturation of AR-LBD in the absence (A and B) or presence (C and D) of DHT. Data collected at 22.5 C are shown. B and D on the *right* display the difference spectra and highlight the change in intensity and red shift in the CM with increasing pressures (from 0–300 MPa). The emission spectra were collected in solutions containing 25 nM AR-LBD and 0.5  $\mu$ M DHT in 50 mM Tris, 2 mM DTT. The samples were excited at  $\lambda_{\text{ex}}$  of 278 nm and emission collected from 300–450 nm through a 1-nm slit for excitation and emission monochromators.

(Table 1). Significantly higher  $\Delta G_u$  and  $\Delta V_u$  in the presence of DHT as compared with the apo-form provides evidence that ligand binding confers energetic stabilization to AR-LBD.

#### Temperature effects on pressure-induced unfolding

From each curve in Fig. 4, the center of mass was calculated using equation 4. The center of mass at 350 MPa (instrument limit) was approximated to the unfolded state ( $\nu_u$ ) and at the ambient pressure to the native folded state ( $\nu_N$ ). The fraction of protein unfolded at each pressure ( $\alpha_p$ ) was calculated using equation 5. The plots used to determine  $\Delta G_u$  and  $\Delta V_u$  at 15 C, 25 C, and 30 C are shown in Fig. 5, A–C, respectively. The lines represent the fits of data to a two-state conformational transition, and the values calculated for the Gibbs free energy and the volume change of the protein upon unfolding are listed in Table 1. The nonlinear dependence of  $\ln K_u$  and therefore  $\Delta G_u$  on temperature indicate that *in vitro* in solution, the protein is more stable at about 25 C. A similar effect of temperature on thermodynamics of unfolding has been reported for Staphylococcal Nuclease and a 23-kDa photosystem protein where the nonlinear behavior was attributed to the increase in heat capacity

**TABLE 1.**  $\Delta G$  and  $\Delta V$  changes associated with unfolding of free and DHT-bound AR-LBD

Temperature (C)	AR-LBD		AR-LBD + DHT	
	$\Delta V$ (ml/mol)	$\Delta G$ (kcal/mol)	$\Delta V$ (ml/mol)	$\Delta G$ (kcal/mol)
15	31.6 $\pm$ 1.1	2.3 $\pm$ 0.2	35.2 $\pm$ 2.7	2.4 $\pm$ 0.4
25	33.8 $\pm$ 1.6	3.5 $\pm$ 0.3	65.7 $\pm$ 2.1	8.4 $\pm$ 0.7
30	17.6 $\pm$ 1.7	2.9 $\pm$ 0.3	38.7 $\pm$ 2.3	4.2 $\pm$ 0.4

These data were derived from the data fits presented in Fig. 5.

upon unfolding (48, 49). At all temperatures, unfolding of DHT-bound LBD resulted in either similar or greater  $\Delta V_u$  as compared with AR-LBD, signifying the ligand-induced compactness in the global protein structure, consistent with the second-derivative absorption and room temperature emission data at ambient pressures.

#### Pressure-induced unfolding of AR-LBD does not dissociate ligand

From the preceding experiments, it was not possible to determine whether the pressure denaturation led to the loss of DHT or DHT stayed associated in the pressure-denatured state. To determine whether the energetics of ligand dissociation from the AR-LBD were contributing to  $\Delta G_u$  and  $\Delta V_u$  measured in pressure-induced unfolding, we performed a series of measurements using a fluorescent androgen analog (Fluormone Al Green, FA). FA binds AR-LBD with a similar affinity as DHT (50, 51). Fluorescence anisotropy of FA was followed as a function of pressure with and without the

AR-LBD. We found that increasing pressure led to a decrease in fluorescence polarization of FA (Fig. 6). In the presence of AR-LBD, steady-state polarization of FA was higher by approximately 90 millipolarization units (mP), consistent with the larger Stokes radius of complexed FA. As pressure was increased, the polarization decreased, but the change in polarization of bound FA was not more than that of free FA (Fig. 6B). We, therefore, conclude that thermodynamic parameters obtained from the pressure-induced unfolding represent the energetics conformational rearrangements in the AR-LBD protein without the loss of DHT. We posit that the pressure induced a denatured state as occurs with chemical denaturation with GnHCl (data not shown), but a reversibly denatured state with ligand still bound.

#### Solvent accessibility probed by partitioning of bis-ANS in AR-LBD with and without DHT

Steady-state emission spectra of bis-ANS were collected in the absence and presence of DHT. Bis-ANS is a nonselective probe that has very low emission in the aqueous environment but displays marked increase in emission in the hydrophobic interior of the protein. Partitioning of bis-ANS has been extensively used to assess solvent accessibility, conformational flexibility, and molten globule states in diverse protein systems (52, 53). Figure 7 displays the emission spectra of bis-ANS (10  $\mu$ M) alone, in presence of AR-LBD (50 nM), and in AR-LBD bound to saturating concentrations of DHT (1  $\mu$ M). Consistent with the second-derivative absorption results, the intensity of bis-ANS emission was lower in the presence of DHT than that in unliganded LBD, suggesting that bis-ANS was excluded from the relatively more compact state in the presence of DHT.

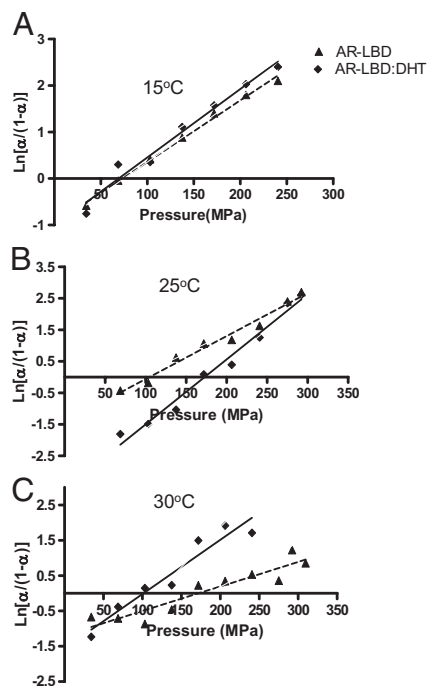


**FIG. 5.** Fits of the extent of unfolding as a function of increasing pressure to evaluate free energy and volume changes in the absence and presence of DHT. Data for  $\lambda_{\text{ex}}$  at 278 nm are shown.  $\alpha$  denotes the fraction of the protein unfolded at each pressure. A–C, Data and fits for unfolding at 15, 25, and 30°C, respectively. Gibbs free energy ( $\Delta G$ ) and molar volume ( $\Delta V$ ) changes associated with unfolding of free and DHT-bound AR-LBD are summarized in Table 1.

In the absence of the AR-LBD, bis-ANS emission spectrum displayed two peaks at 495 and 536 nm. Upon addition of AR-LBD, the emission intensity as well as spectrum of bis-ANS changed substantially. Consistent with the partitioning of the probe inside the protein, the  $\lambda_{495}/\lambda_{536}$  ratio increased from 0.8 to 1.3.

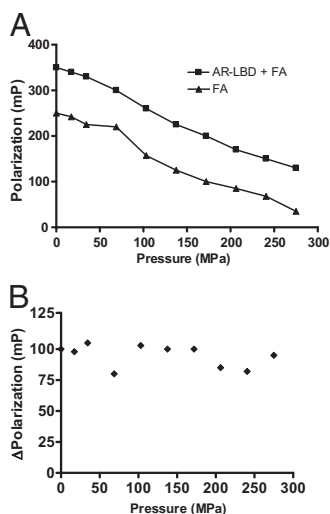


**FIG. 6.** A, Effect of pressure on the polarization of FA with and without AR-LBD. FA (2 nm) was incubated with 25 nM AR-LBD in 50 mM Tris and 2 mM DTT for 1 h before the pressure titration. The experiments were conducted at 22°C, and the solution was allowed to equilibrate at each pressure for 5 min before data acquisition. B, Difference between the polarization of FA with and without AR-LBD at each point during pressurization.  $\Delta mP$  is the corresponding difference in two polarization measurements.

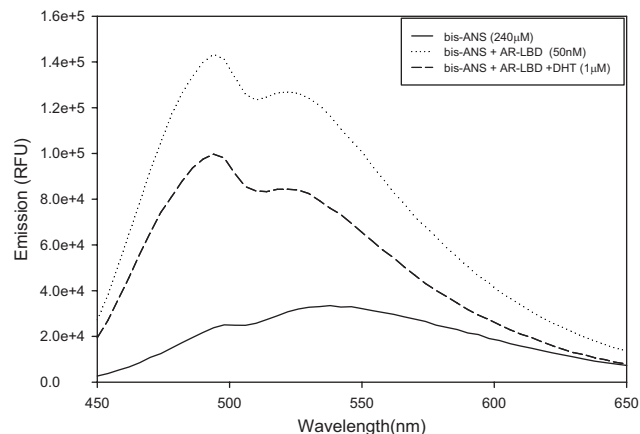


**FIG. 7.** Effect of AR-LBD with and without DHT on the emission properties of nonselective probe bis-ANS. Bis-ANS (10  $\mu\text{M}$ ) was incubated with 50 nM AR-LBD with or without saturating concentrations of DHT (1  $\mu\text{M}$ ).  $\lambda_{\text{ex}}$  was set at 395 nm, and emission was collected from 430–610 nm.

### Kinetics of DHT-induced conformational changes in AR-LBD

We used stopped-flow mixing to examine the transient kinetics of DHT-induced conformational changes using bis-ANS as a nonspecific probe. Interestingly, we found that the protein underwent a biphasic rearrangement with an initial fluorescence increase ( $k_{\text{obs}} = 30 \text{ sec}^{-1}$ ) that was followed by a slow decrease in fluorescence ( $k_{\text{obs}} = 0.01 \text{ sec}^{-1}$ ) (Fig. 8A). The initial phase resulted in an increase in solvent accessibility to the interior of the protein as indicated by the rapid rise in bis-ANS emission. This is consistent with a molten globule-like structure that reflects overall rearrangement in AR-LBD in response to DHT binding. This open conformational state subsequently collapsed into a more stable, conformationally compact state where bis-ANS was excluded and resulted in an eventual drop in emission intensity below the unliganded protein (Fig. 8). To eliminate the effects of photobleaching of bis-ANS and because we observed a large decrease in fluorescence from mixing AR-LBD with buffer alone, we also examined the ligand-induced fluorescence transients after subtracting the buffer control transient. There was no change in the rate constants of the initial fluorescence increase, but the slow decrease was altered by the subtraction ( $k_{\text{obs}} = 0.01 \text{ sec}^{-1}$ ). We further examined the concentration and temperature dependence of the initial fluorescence increase. We found that the rate constant was independent of DHT concentration, ascertaining that this phase was protein rearrangement and not a convolution of bimolecular ligand-receptor binding event (Fig. 8B). From the temperature dependence of conformational rearrangement within the liganded AR-LBD, the activation energy barrier ( $\Delta E_{\text{act}}$ ) was calculated to be 13.4 kcal/mol (Fig. 8C).

### Dynamics of AR-LBD rearrangement probed by molecular dynamics simulations

We conducted a series of molecular dynamics studies to follow rearrangement of specific residues and fragments within the AR-LBD. The starting structure for simulations of the AR apo-form was obtained by removing the ligand from the agonist-bound crystal structure (PDB ID 1QX30) and rotating the helix

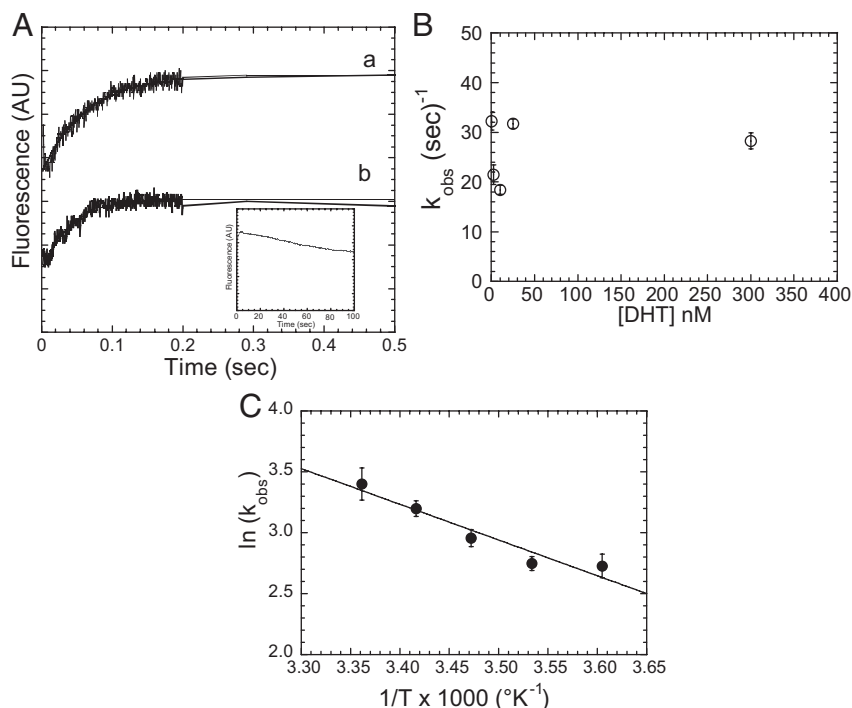


**FIG. 8.** Concentration and temperature dependence of DHT-induced conformational changes in the AR-LBD. A, Fluorescence transients from mixing 5 nM AR-LBD with 100  $\mu$ M DHT and the single exponential fits to the data. The top trace (a) was taken at 10 C, and the bottom trace (b) was taken at 20 C ( $k_{obs} = 15.6 \pm 0.5$  and  $24.5 \pm 0.8$  sec<sup>-1</sup>, respectively). The inset shows the slow decrease observed over a 100-sec time scale after subtracting the buffer control ( $k_{obs} = 0.01 \pm 0.001$  sec<sup>-1</sup>). B, Independence of the rate constants on DHT concentration for the initial faster component examined at 22.5 C. C, Arrhenius plots that demonstrate the temperature dependence of the initial faster component and the linear fit of the data that was used to determine the Arrhenius activation energy. Error bars represent SE of the fits at each temperature.

12 away from the ligand-binding pocket as described in *Materials and Methods*. Simulations of both ligand-bound and apo-form structures were conducted for 10 nsec using AMBER force field (*cf. Materials and Methods*). Specifically, we wanted to 1) examine whether the pressure-induced unfolding pathways were distinct between the ligand-bound and apo-AR-LBD and 2) follow the dynamics of rearrangement in coactivator binding surfaces and the hydrophobic cleft formed by the helices 3, 3', 4, 5, and 12.

Structural alignments of initial AR LBD ligand-bound and apo-form structures (*pink coloring*) with the corresponding structures extracted after 10 nsec of unrestrained simulations at physiological conditions (*pale green coloring*) are shown in Fig. 9, A and B. One sees that although there were insignificant structural changes in the ligand-bound structure, the apo-form AR-LBD underwent more noticeable conformational shifts in several regions with the most significant one being alteration of helix 12, as expected. In Fig. 9C, the AR LBD apo-form cartoon is colored according to the difference between residue root mean square deviation (RMSD) in ligand-bound and apo-form structures calculated over the time course of 10 nsec. Virtually all residues of the apo-form structure exhibit increased mobility as compared with the ligand-bound protein and, unexpectedly, the most significant changes in mobility are found far from the ligand-binding pocket.

We followed the total solvent-accessible surface areas (ASAs) for Trp and Tyr residues as functions of time during the course

of a simulation up to 10 nsec for ligand-bound and ligand-free forms for two pressure values: atmospheric and 350 MPa (50 kPsi). We found that in ligand-bound protein, the elevated pressure results in a gradual increase of Trp ASA while Tyr residues remain buried, whereas in the apo-form protein, it is the Tyr ASA that is being increased (data not shown). These findings are consistent with the experimental data generated by pressure-perturbation experiments and suggest that distinct conformational states are populated during unfolding, depending on whether the ligand is bound or not.

Next we examined the conformational rearrangement in the specific sets of residues of AR-LBD that participate in ligand binding and coactivator recruitment. Figure 9D shows RMSDs of particular groups of residues: ligand-binding interface (LBI), coactivator recruitment surface 1 (CoaRS1), CoaRS2, coactivator binding cleft (CoaBC), and everything except coactivator binding cleft (non-CoaBC). As expected, the residues within LBI display conformational rearrangement in response to the ligand removal. Additionally, we observed that CoaRS2, which encompasses the functionally important AF2 region in AR-LBD, exhibits noticeable conformational change and increased mobility in the ligand-free structure. Within the modeling constraints, we do not see substantial conformational changes in CoaRS1 comprised of V713, V730, and M734, although it has been shown to play role in modulating ligand dissociation.

## Discussion

We used a combination of emission and absorption spectroscopy to examine the kinetics and thermodynamics of DHT-induced conformational stabilization in AR-LBD; both indicate that upon ligand binding, there was an increase in the hydrophobic environment of tyrosine and tryptophan residues within a more compact DHT-bound protein. Consistent with the partial proteolysis and pull-down assays (8, 19–31), our molecular modeling studies suggest that residues in AF2 are quite sensitive to the ligand-receptor interactions. Nonspecific interactions of bis-ANS with the AR-LBD demonstrate that the dye is excluded from the interior of the protein upon ligand binding. Our kinetic data show that these rearrangements display an interesting biphasic behavior; a rapid burst phase ( $k_{obs} = \sim 30$  sec<sup>-1</sup>) that allows greater partitioning of bis-ANS in the protein is followed by a slower rearrangement that pushes the dye out of the hydrophobic pockets. Thus, DHT association induces the AR-LBD to acquire an intermediate state that is partially unfolded. Such partially unfolded intermediate states have been sug-

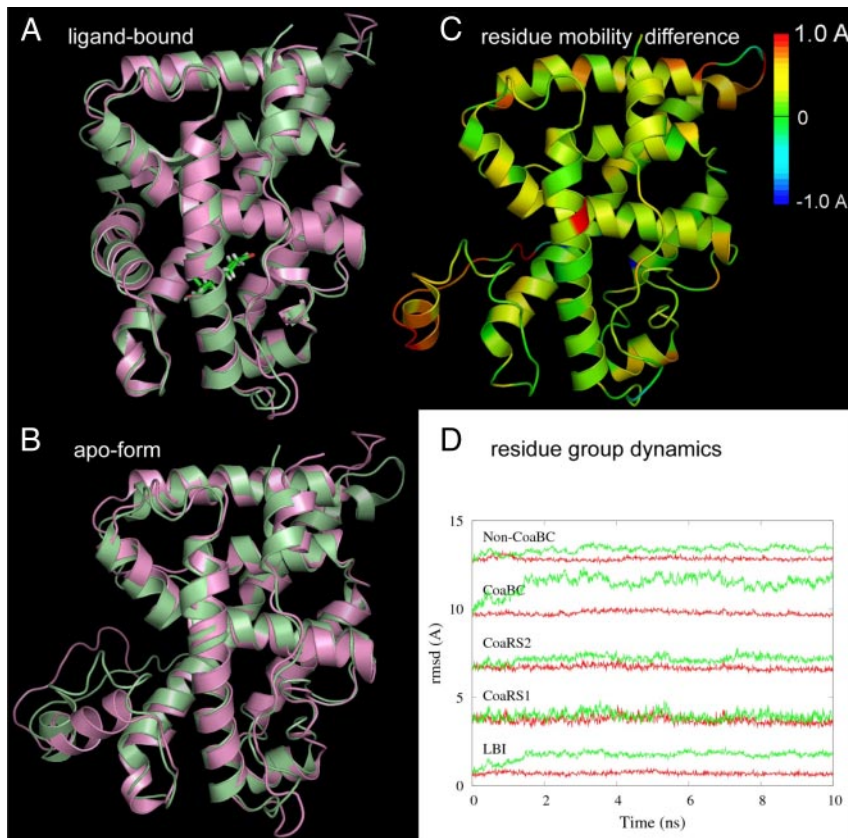


**FIG. 9.** Molecular dynamics simulations of the AR-LBD at a temperature of 295.5 K and atmospheric pressure. A and B, Superimposed cartoon representations of AR-LBD in the ligand-bound form and apo-form, respectively. *Pink coloring* represents initial structures, and *pale green coloring* represents structures after 10 nsec of simulations. C, AR-LBD apo-form colored by the difference between  $\sigma$  of residue RMSDs for LBD-R1881 complex and apo-form (*i.e.* by changes in residue mobilities upon ligand unbinding) over a 6- to 10-nsec time interval. Positive values correspond to greater mobility in the apo-form. D, Predicted RMSDs for LBI, CoaRS1, CoaRS2, and CoaBC. *Red curves* show RMSDs of helices in a ligand-bound structure, whereas *green curves* show them in an apo-form structure. The groups of residues are defined as follows: LBI (V685, L701, N705, L707, Q711, L744, M745, M749, R752, Y763, F764, Q783, M787, F876, T 877, L880, F891, and M895), CoaRS1 (V713, V730, and M734), CoaRS2 (E709, L712, V713, V715, V716, K717, K720, F725, R726, V730, Q733, M734, I737, and Q738), CoaBC (helices 3, 3', 4, 5, and 12), and non-CoaBC (helices 1, 6, 7, 8, 9, 10, and 11).

gested to play an important role in the coactivator/repressor recruitment in the sequence of events associated with ligand entry into and exit from the binding pocket of AR-LBD. Similar molten globule states that are transiently populated have been reported in estrogen and estrogen receptor interactions (34).

Although the finding that DHT binding leads to a more compact structure and stabilizes the AR-LBD against pressure-induced denaturation is not surprising, our data revealed that ligand binding has stabilizing effects on some residues that are remote from the site of ligand binding and that are involved in forming the coactivator binding groove. This may partly explain how subtle changes in ligand structure [antagonist/selective androgen receptor modulator (SARM) classes] that elicit selectivity in coregulator interaction. Within the range of pressure increases that were possible, the protein attains an intermediate, partially unfolded state where the ligand-binding pocket still retains its structure. The volume changes that accompany the transition to this conformational state are greater in amplitude when the DHT-bound structure is unfolded. The absolute val-

ues of volume changes ( $\Delta V$ ) are small ( $\sim 20$ – $60$  ml/mol) due to compensatory contributions of intrinsic volume ( $\Delta V_M$ ), void volume created at the interface of solvent and protein from the thermally activated mutual vibrations ( $\Delta V_T$ ), and interaction volume that arises from the solvent contraction ( $\Delta V_I$ ). The individual contributions from these volume components is usually large but of opposing signs.  $\Delta V_M$  and  $\Delta V_I$  decrease as proteins unfold, but the  $\Delta V_T$  increases to an extent dependent on the nature of residues exposed to the solvent. We posit that in AR-LBD, a small  $\Delta V$  is a result of the compensation among these parameters.

At steady state, increased Bis-ANS partitioning into the unliganded protein suggests a flexible, more solvent-accessible AR-LBD. Our data suggest that unliganded AR-LBD is in a dynamic equilibrium between multiple conformational states and may explain the difficulties involved in obtaining a crystal structure of the apo-form. In addition, the flexible structure of unliganded AR may not allow high-affinity interaction with coactivator/corepressors.

Dynamics of bis-ANS partitioning upon ligand binding reveals an interesting biphasic nature of receptor rearrangement. A transient, molten globule-like state with increased solvent accessibility (and probably a more disordered state) gives rise to a more compact state with a significant exclusion of the bis-ANS (and therefore solvent) from the protein interior. The DHT-bound state at equilibrium is conformationally a more compact and energetically stable state. This feature may allow AR to gate the signaling depending on the ligand-specific conformation.

The computational modeling and spectroscopic measurements show that intrinsic Tyr and Trp residues provide a sensitive tool to examine the dynamics of conformational rearrangement upon ligand binding. Molecular modeling studies suggest distinct unfolding pathways in the presence or absence of agonist. We found that removal of ligand causes dramatic rearrangement in regions that are distant from the ligand-binding pocket and that make up the hydrophobic cleft. This region, encompassed by the helices 3, 3', 5, 7, and 12, is functionally important in recruiting critical coactivators of the steroid receptor coactivator, receptor-interacting protein, thyroid hormone receptor-associated protein, and heat-shock protein 70 families.

Similar conformational dynamics have also been observed in other nuclear hormone receptors. Using nuclear magnetic resonance spectroscopy, Johnson *et al.* (54) found that unbound peroxisome proliferator-activated receptor- $\gamma$  displays a high de-

gree of flexibility that collapses into a well-defined structural state in the presence of ligand. It was suggested that this loss in conformational entropy in liganded form plays an important role in coactivator binding efficiency. Similarly, using the non-specific probe bis-ANS, estrogen receptor was shown to populate a molten globule state during denaturant-induced unfolding (53). A recent study of P160 coactivator (ACTR) peptide binding to cAMP response element-binding protein-binding protein (CBP) residues displays interesting synergistic rearrangement where the globular form of unbound CBP thermodynamically regulates the protein-protein interaction (55). Elegant studies using peptide phage display (30, 31) and a recent study with synthetic nonsteroidal SARM also have suggested that SARMS might populate a conformation that is distinct from the agonist-bound form in the energy coordinate capable of selective recruitment of coregulators (56).

This study is the first step in examining the molecular basis of potency and selectivity in ligand-specific AR action. We posit that agonist-bound structures are capable of binding coactivators by populating a distinct set of conformations in the spatial coordinates when compared with antagonists. The SARMS, on the other hand, either populate a different set of conformational structures or alter the activation energy ( $\Delta E_{act}$ ) between the agonist- and antagonist-bound states, thereby modulating the selectivity and relative potency of androgen's effects. The biophysical parameters characterized in this study provide unique insights into the thermodynamics and kinetics of ligand-receptor interactions that cannot be obtained from partial proteolysis and pull-down assays. The complementary use of these spectroscopic techniques along with molecular biology studies and biochemical assays can help test the hypothesis that ligands modulate  $\Delta E_{act}$  and  $\Delta G$ , thereby regulating the extent of partitioning of receptor in distinct conformational states, which in turn may determine the potency of coregulator recruitment and transcriptional activation.

## Materials and Methods

### Protein and ligand

Purified AR-LBD [His-glutathione S-transferase (GST)-LBD] and Fluormone AL green were obtained from Invitrogen, Inc. (San Diego, CA). The effective protein concentration was calculated from the specific activity evaluated by the vendor (purity >85%). This construct has been previously characterized for its ligand binding and coregulator recruitment, which are similar to those of the full-length receptor from LNCaP lysates (51, 57). In addition, we found that addition of DHT to the purified GST did not alter the emission properties so we conclude that the presence of a GST tag does not elicit significant perturbation on ligand-receptor interaction. Nevertheless, we have limited our inferences to ligand-induced changes rather than absolute values of these variables.

DHT was obtained from Sigma Chemical Co. (St. Louis, MO), and DHT stocks were prepared in ethanol. During titrations, the ethanol concentrations were kept below 0.5%. All the spectroscopic measurements were conducted in 50 mM Tris buffer at pH 7.4 with 2 mM dithiothreitol (DTT). AR-LBD was further characterized by constructing Perrin plots. Steady-state fluorescence anisotropy was examined using a Photon Technology International (Birmingham, NJ) fluorimeter equipped with excitation/emission polarizers and monochromator. The fluorescence lifetimes were determined by time-

correlated single-photon counting using a picosecond N<sub>2</sub> dye laser as an excitation source and examining the emitted fluorescence decay using an emission monochromator. Lifetime decays were fit with custom software provided with the Photon Technology International instrument. We calculated the limiting anisotropy ( $r_0$ ) and rotational correlation time ( $\phi$ ) by examining the steady-state anisotropy as a function of solvent viscosity by varying the glycerol concentration at constant temperature (10, 20, and 30 C). Glycerol was varied from 10–40% (wt/wt) and did not affect the emission spectrum or fluorescence lifetimes. The  $r_0$  and  $\phi$  were determined from the linear fit of the anisotropy as a function of viscosity plots (58):

$$1/r = 1/r_0 + \tau/(r_0\phi) \quad (1)$$

The data were corrected for fraction of FA bound to AR-LBD, and the average lifetime was found to be 3.5 nsec for the free and bound FA. The rotational correlation time is related to the molecular weight of the free FA or FA/AR-LBD complex by the following equation

$$\phi = V\eta/(RT) = M(\nu + b)\eta/RT \quad (2)$$

where  $V$  is the volume of the sphere,  $\eta$  is the viscosity,  $R$  is the gas constant,  $T$  is the temperature,  $M$  is the molecular weight,  $\nu$  is the specific volume, and  $b$  is the hydration. Assuming a specific volume of 0.73 ml/g and a hydration of 0.23 g H<sub>2</sub>O/g protein or ligand, the molecular weight can be estimated.

### Steady-state, second-derivative absorption

Absorption and difference spectra were recorded on a Beckman DU-800 spectrophotometer. Second-derivative spectra were obtained using the software package provided by the manufacturer. Determination of residue exposure in the protein by second-derivative spectroscopy was carried out as described previously (43–47). The second-order differential equations calculations do not impact the Beer-Lambert law; therefore, the a/b ratio can be depicted as follows:

$$\frac{\alpha}{\beta} = \frac{\left(\frac{d^2}{d\lambda^2} Abs_1(\lambda)\right)}{\left(\frac{d^2}{d\lambda^2} Abs_2(\lambda)\right)} = \frac{\delta\left[\frac{\epsilon_1 Tyr}{\epsilon_2 Trp}\right]_n + \delta\left[\frac{\epsilon_1 Trp}{\epsilon_2 Tyr}\right]_n}{\delta\left[\frac{\epsilon_2 Tyr}{\epsilon_2 Trp}\right]_n + 1} \quad (3)$$

where the ratio of the extinction coefficients on the right side of the equation is the difference in second-order derivatives at two fixed pairs of wavelengths (subscript 1, 278/273; subscript 2, 287/282).

### Steady-state fluorescence measurements and high-pressure denaturation

Fluorescence spectroscopy was carried out with ISS-K2 (Champaign, IL) equipment. Polarization measurements with the Fluormone AL Green were carried out in T format. The temperature was equilibrated with a VWR circulating bath attached to the cuvette holder. At low temperatures, the nitrogen gas was circulated around the cuvette and the pressure cell windows to prevent condensation. Fluorescence measurements under pressure were performed using a high-pressure bomb described by Paladini and Weber (59, 60), fitted with sapphire windows, and adapted to the ISS-K2 fluorimeter. The temperature inside the sample holder was maintained at 22 C by using a thermostat, unless otherwise specified. The changes in spectral area, fluorescence intensity, and CM were monitored as a function of pressure. The CM was calculated from integrated emission curves as:

$$\nu = \frac{\sum \nu_i F_i}{\sum F_i} \quad (4)$$

where  $\nu$  is the center of mass in wave numbers,  $F_i$  is the fluorescence emitted at wave number  $\nu_i$ . To describe the denaturation process, we used the shifts in CM due to pressure to compute the fraction of denatured species at each pressure ( $\alpha_p$ ) according to Weber (60).

The fraction of unfolded receptor ( $\alpha$ ) was calculated with the assumption that CM at atmospheric pressure represents completely folded state  $\nu_u$  and at 350 mPa represented the unfolded state  $\nu_u$  (61–63):

$$\alpha_p = \frac{1}{1 + Q \left( \frac{\nu_p - \nu_u}{\nu_f - \nu_p} \right)} \quad (5)$$

where  $\nu_p$  is the CM at a given pressure. Thermodynamic parameters for the pressure unfolding for a unimolecular transition were determined according to equation 6:

$$\ln \left[ \frac{\alpha_p}{(1 - \alpha_p)} \right] = p \left( \frac{\Delta V_p}{RT} \right) + \ln K_u \quad (6)$$

where  $\Delta V_u$  is the volume change and  $K_u$  is the equilibrium constant for pressure unfolding extrapolated to atmospheric pressure (62, 63).

### Transient kinetics

Kinetic measurements were made using an Applied Photophysics (Leatherhead, Surrey UK) SX18MV stopped-flow spectrophotometer with an instrument dead time of 1.2 msec. The bis-ANS fluorescence was excited at 395 nm, and the emission was monitored using a 420-nm long pass filter. At least three shots were averaged before fitting the kinetic transients. Nonlinear least-squares fitting of the data was done with software provided with the instrument or KaleidaGraph (Synergy Software) (Reading, PA). Uncertainties reported are SE of the fits unless stated otherwise.

### Molecular dynamics simulations

Molecular dynamics simulations of the ligand-bound AR-LBD were performed in explicit solvent using a parallel, object-oriented molecular dynamics program (NAMD) (64), starting from a crystallographically determined structure (PDB entry 1XQ3). Six missing residues were reconstructed using MOE homology modeling module (Chemical Computing Group). Crystallographically determined water molecules were removed except the one in the ligand-binding pocket. The protein and solvent were described by the Amber99 force field (65), whereas the ligand was described by General Amber Force Field (GAFF) (66). The force field parameters for ligand were derived using the Antechamber module of the Amber package (67), and the complex was then built using the tLEaP module. The complex was solvated with 13,521 TIP3P water molecules and neutralized with 5 Cl<sup>-</sup> ions. The final complex consisting of 44,715 atoms was minimized for 2500 steps with backbone and ligand atoms fixed, 2500 steps with backbone and ligand atoms restrained by harmonic potential with spring constant of 1.0 kcal/mol · Å, and subsequently twice for 2500 steps reducing the spring constant by a factor of two. The system was heated using Langevin dynamics under the NPT ensemble using Langevin Piston pressure control, during 10 psec with harmonic restraints of 1.0 kcal/mol · Å applied to Ca atoms. It was then equilibrated with same Ca restraints for 40 psec, for another 40 psec with 0.5 kcal/mol · Å restraints, for 5 psec with 0.25 kcal/mol · Å restraints, and 5 psec unrestrained. The system was then subjected to unrestrained molecular dynamics simulation during 10 nsec in the NPT ensemble.

Because of the absence of crystallographic or nuclear magnetic resonance structure data for the AR-LBD in its apo-form, a computational model for the initial apo-form structure has to be employed in simulations. Generation of a model representing an adequate approximation to the apo-form structure is a critical and challenging step. Given rather low sequence identity to other known nuclear receptor apo-form structures (e.g. 1LBD), we have concluded that homology modeling would not provide sufficiently adequate description. Rather, we have generated a starting structure based on the 1XQ3 structure (cf. Fig. 9A), where the ligand was removed from the PDB file and helix 12 was rotated away from the ligand-binding pocket using the PyMol (68) sculpting tool. The resulting structure (cf. Fig. 9B) was used as a starting structure in simulations of the apo-form AR-LBD. We believe that time

evolution of such a structure, with ligand-binding pocket and H12 helix being substantially exposed to solvent, may provide a better description of the AR-LBD dynamics in its apo-form. Trajectory analyses including RMSD calculations were performed using visual molecular dynamics (69). Solvent ASAs of Trp and Tyr residues were calculated by the DSSP approach (70).

### Acknowledgments

Address all correspondence and requests for reprints to: Dr. Ravi Jasuja, Muscle and Aging Research Unit, Boston University School of Medicine, Section of Endocrinology, Diabetes, and Nutrition, Boston, Massachusetts 02199. E-mail: jasuja@bu.edu.

This work was supported by the following grants: National Institute of Child Health and Human Development Grant 5U54HD041748-sub-project (R.J.), National Institute on Aging Grant 1U01AG14369 supplement (to R.J. and S.B.), National Institute of Diabetes and Digestive and Kidney Diseases Grant 1R01DK70534 (to S.B.), and National Institute of General Medical Sciences Grant R01GM073082 (to A.Y.I., D.R.L., and D.J.J.).

Disclosure Summary: The authors have nothing to declare.

### References

1. Quigley CA, De Bellis A, Marschke KB, el-Awady MK, Wilson EM, French FS 1995 Androgen receptor defects: historical, clinical, and molecular perspectives. *Endocr Rev* [Erratum (1995) 16:546] 16:271–321
2. Brinkmann AO, Klaasen P, Kuiper GG, van der Korput JA, Bolt J, de Boer W, Smit A, Faber PW, van Rooij HC, Geurts van Kessel A, Mulder E, Trapman J 1989 Structure and function of the androgen receptor. *Urol Res* 17:87–93
3. Gobinet J, Poujol N, Sultan Ch 2002 Molecular action of androgens. *Mol Cell Endocrinol* 198:15–24
4. Bhasin S, Cunningham GR, Hayes FJ, Matsumoto AM, Snyder PJ, Swerdloff RS, Montori VM 2006 Testosterone therapy in adult men with androgen deficiency syndromes: an endocrine society clinical practice guideline. *J Clin Endocrinol Metab* 91:1995–2010
5. Bhasin S 2007 Testicular disorders. In: Kronenberg H, Polonsky KS, Larsen PR, Melmed S, eds. *Williams' textbook of endocrinology*. 11th ed. New York: Elsevier Health Sciences
6. Gelmann EP 2002 Molecular biology of the androgen receptor. *J Clin Oncol* 20:3001–3015
7. Kuil CW, Mulder E 1995 Effects of androgens and antiandrogens on the conformation of the androgen receptor. *Ann NY Acad Sci* 761:351–354
8. Tyagi RK, Lavrovsky Y, Ahn SC, Song CS, Chatterjee B, Roy AK 2000 Dynamics of intracellular movement and nucleocytoplasmic recycling of the ligand-activated androgen receptor in living cells. *Mol Endocrinol* 14:1162–1174
9. Kuil CW, Mulder E 1994 Mechanism of antiandrogen action: conformational changes of the receptor. *Mol Cell Endocrinol* 102:R1–R5
10. Kempainen JA, Lane MV, Sar M, Wilson EM 1992 Androgen receptor phosphorylation, turnover, nuclear transport, and transcriptional activation. Specificity for steroids and antihormones. *J Biol Chem* 267:968–974
11. Trapman J, Ris-Stalpers C, van der Korput JA, Kuiper GG, Faber PW, Romijn JC, Mulder E, Brinkmann AO 1990 The androgen receptor: functional structure and expression in transplanted human prostate tumors and prostate tumor cell lines. *J Steroid Biochem Mol Biol* 37:37–42
12. Williams SP, Sigler PB 1998 Atomic structure of progesterone complexed with its receptor. *Nature* 393:392–396
13. Evans RM 1988 The steroid and thyroid hormone receptor superfamily: transcriptional regulators of development and physiology. *Science* 240:889–895
14. Kumar R, Thompson EB 1999 The structure of the nuclear hormone receptors. *Steroids* 64:310–319
15. Roy AK, Tyagi RK, Song CS, Lavrovsky Y, Ahn SC, Oh TS, Chatterjee B 2001 Androgen receptor: structural domains and functional dynamics after ligand-receptor interaction. *Ann NY Acad Sci* 949:44–57
16. Tan JA, Joseph DR, Quarby VE, Lubahn DB, Sar M, French FS, Wilson EM 1988 The rat androgen receptor: primary structure, autoregulation of its messenger ribonucleic acid, and immunocytochemical localization of the receptor protein. *Mol Endocrinol* 2:1276–1285
17. Jenster G, van der Korput HA, van Vroonhoven C, van der Kwast TH, Trapman J, Brinkmann AO 1991 Domains of the human androgen receptor

- involved in steroid binding, transcriptional activation, and subcellular localization. *Mol Endocrinol* 5:1396–1404
18. Trapman J, Klaassen P, Kuiper GG, van der Korput JA, Faber PW, van Rooij HC, Geurts van Kessel A, Voorhorst MM, Mulder E, Brinkmann AO 1988 Cloning, structure and expression of a cDNA encoding the human androgen receptor. *Biochem Biophys Res Commun* 153:241–248
  19. Askew EB, Gampe Jr RT, Stanley TB, Faggart JL, Wilson EM 2007 Modulation of androgen receptor activation function 2 by testosterone and dihydrotestosterone. *J Biol Chem* 282:25801–25816
  20. He B, Kempainen JA, Voegel JJ, Gronemeyer H, Wilson EM 1999 Activation function 2 in the human androgen receptor ligand binding domain mediates interdomain communication with the NH<sub>2</sub>-terminal domain. *J Biol Chem* 274:37219–37225
  21. He B, Gampe Jr RT, Hnat AT, Faggart JL, Minges JT, French FS, Wilson EM 2006 Probing the functional link between androgen receptor coactivator and ligand-binding sites in prostate cancer and androgen insensitivity. *J Biol Chem* 281:6648–6663
  22. Hur E, Pfaff SJ, Payne ES, Grøn H, Buehrer BM, Fletterick RJ 2004 Recognition and accommodation at the androgen receptor coactivator binding interface. *PLoS Biol* 2:E274–E279
  23. He B, Minges JT, Lee LW, Wilson EM 2002 Dependence of selective gene activation on the androgen receptor NH<sub>2</sub>- and COOH-terminal interaction. *J Biol Chem* 277:10226–10235
  24. Heinlein A, Chang C 2002 Androgen receptor (AR) coregulators: an overview. *Endocr Rev* 23:157–200
  25. Shibata H, Spencer TE, Onate SA, Jenster G, Tsai SY, Tsai MJ, O'Malley BW 1997 Role of co-activators and co-repressors in the mechanism of steroid/thyroid receptor action. *Recent Prog Horm Res* 52:141–164; discussion 164–165
  26. He B, Wilson EM 2003 Electrostatic modulation in steroid receptor recruitment of LXXLL and FXXLF motifs. *Mol Cell Biol* 23:2135–2150
  27. Kazmin D, Prytkova T, Cook CE, Wolfinger R, Chu TM, Beratan D, Norris JD, Chang CY, McDonnell DP 2006 Linking ligand-induced alterations in androgen receptor structure to differential gene expression: a first step in the rational design of selective androgen receptor modulators. *Mol Endocrinol* 20:1201–1217
  28. van de Wijngaert DJ, van Royen ME, Hersmus R, Pike AC, Houtsmuller AB, Jenster G, Trapman J, Dubbink HJ 2006 Novel FXXXFF and FXXMF motifs in androgen receptor cofactors mediate high affinity and specific interactions with the ligand-binding domain. *J Biol Chem* 281:19407–19416
  29. Smith CL, O'Malley BW 2004 Coregulator function: a key to understanding tissue specificity of selective receptor modulators. *Endocr Rev* 25:45–71
  30. Chang CY, McDonnell DP 2002 Evaluation of ligand-dependent changes in AR structure using peptide probes. *Mol Endocrinol* 16:647–660
  31. Chang CY, Abdo J, Hartney T, McDonnell DP 2005 Development of peptide antagonists for the androgen receptor using combinatorial peptide phage display. *Mol Endocrinol* 19:2478–2490
  32. Hong H, Darimont BD, Ma H, Yang L, Yamamoto KR, Stallcup MR 1999 An additional region of coactivator GRIP1 required for interaction with the hormone-binding domains of a subset of nuclear receptors. *J Biol Chem* 274:3496–3502
  33. Ding XF, Anderson CM, Ma H, Hong H, Uht RM, Kushner PJ, Stallcup MR 1998 Nuclear receptor-binding sites of coactivators glucocorticoid receptor interacting protein 1 (GRIP1) and steroid receptor coactivator 1 (SRC-1): multiple motifs with different binding specificities. *Mol Endocrinol* 12:302–313
  34. Tamrazi A, Carlson KE, Rodriguez AL, Katzenellenbogen JA 2005 Coactivator proteins as determinants of estrogen receptor structure and function: spectroscopic evidence for a novel coactivator-stabilized receptor conformation. *Mol Endocrinol* 19:1516–1528
  35. Hurth KM, Nilges MJ, Carlson KE, Tamrazi A, Belford RL, Katzenellenbogen JA 2004 Ligand-induced changes in estrogen receptor conformation as measured by site-directed spin labeling. *Biochemistry* 43:1891–1907
  36. Jenster G, Spencer TE, Burcin MM, Tsai SY, Tsai MJ, O'Malley BW 1997 Steroid receptor induction of gene transcription: a two-step model. *Proc Natl Acad Sci USA* 94:7879–7884
  37. Sack JS, Kish KF, Wang C, Attar RM, Kiefer SE, An Y, Wu GY, Scheffler JE, Salvati ME, Krystek Jr SR, Weinmann R, Einspahr HM 2001 Crystallographic structures of the ligand-binding domains of the androgen receptor and its T877A mutant complexed with the natural agonist dihydrotestosterone. *Proc Natl Acad Sci USA* 98:4904–4909
  38. Pereira de Jésus-Tran K, Côté PL, Cantin L, Blanchet J, Labrie F, Breton R 2006 Comparison of crystal structures of human androgen receptor ligand-binding domain complexed with various agonists reveals molecular determinants responsible for binding affinity. *Protein Sci* 15:987–999
  39. Bohl CE, Wu Z, Miller DD, Bell CE, Dalton JT 2007 Crystal structure of the T877A human androgen receptor ligand-binding domain complexed to cyproterone acetate provides insight for ligand-induced conformational changes and structure-based drug design. *J Biol Chem* 282:13648–13655
  40. Estébanez-Perpiñá E, Arnold LA, Arnold AA, Nguyen P, Rodrigues ED, Mar E, Bateman R, Pallai P, Shokat KM, Baxter JD, Guy RK, Webb P, Fletterick RJ 2007 A surface on the androgen receptor that allosterically regulates co-activator binding. *Proc Natl Acad Sci USA* 104:16074–16079
  41. Bohl CE, Gao W, Miller DD, Bell CE, Dalton JT 2005 Structural basis for antagonism and resistance of bicalutamide in prostate cancer. *Proc Natl Acad Sci USA* 102:6201–6206
  42. Feng W, Ribeiro RC, Wagner RL, Nguyen H, Apriletti JW, Fletterick RJ, Baxter JD, Kushner PJ, West BL 1998 Hormone-dependent coactivator binding to a hydrophobic cleft on nuclear receptors. *Science* 280:1747–1749
  43. Ragone R, Colonna G, Balestrieri C, Servillo L, Irace G 1984 Determination of tyrosine exposure in proteins by second-derivative spectroscopy. *Biochemistry* 23:1871–1875
  44. Servillo L, Colonna G, Balestrieri C, Ragone R, Irace G 1982 Simultaneous determination of tyrosine and tryptophan residues in proteins by second-derivative spectroscopy. *Anal Biochem* 126:251–257
  45. Kuelz LA, Ersoy B, Ralston JP, Middaugh CR 2003 Derivative absorbance spectroscopy and protein phase diagrams as tools for comprehensive protein characterization: a bGCSF case study. *J Pharm Sci* 92:1805–1820
  46. Mach H, Middaugh CR 1994 Simultaneous monitoring of the environment of tryptophan, tyrosine, and phenylalanine residues in proteins by near-ultraviolet second-derivative spectroscopy. *Anal Biochem* 222:323–331
  47. Mach H, Thomson JA, Middaugh CR 1989 Quantitative analysis of protein mixtures by second derivative absorption spectroscopy. *Anal Biochem* 181:79–85
  48. Panick G, Malessa R, Winter R, Rapp G, Frye KJ, Royer CA 1998 Structural characterization of the pressure-denatured state and unfolding/refolding kinetics of staphylococcal nuclease by synchrotron small-angle x-ray scattering and Fourier-transform infrared spectroscopy. *J Mol Biol* 275:389–402
  49. Li Y, Jing G 2000 Double point mutant F34W/W140F of staphylococcal nuclease is in a molten globule state but highly competent to fold into a functional conformation. *J Biochem* 128:739–744
  50. Jasuja R, Catlin DH, Miller A, Chang YC, Herbst KL, Starcevic B, Artaza JN, Singh R, Datta G, Sarkissian A, Chandsawangbhuwana C, Baker M, Bhasin S 2005 Tetrahydrogestrinone is an androgenic steroid that stimulates androgen receptor-mediated, myogenic differentiation in C3H10T1/2 multipotent mesenchymal cells and promotes muscle accretion in orchidectomized male rats. *Endocrinology* 146:4472–4478
  51. Le HT, Schaldach CM, Firestone GL, Bjeldanes LF 2003 Plant-derived 3,3'-diindolylmethane is a strong androgen antagonist in human prostate cancer cells. *J Biol Chem* 278:21136–21145
  52. Celej MS, Montich GG, Fidelio GD 2003 Protein stability induced by ligand binding correlates with changes in protein flexibility. *Protein Sci* 12:1496–1506
  53. Gee AC, Katzenellenbogen JA 2001 Probing conformational changes in the estrogen receptor: evidence for a partially unfolded intermediate facilitating ligand binding and release. *Mol Endocrinol* 15:421–428
  54. Johnson BA, Wilson EM, Li Y, Moller DE, Smith RG, Zhou G 2000 Ligand-induced stabilization of PPAR $\gamma$  monitored by NMR spectroscopy: implications for nuclear receptor activation. *J Mol Biol* 298:187–194
  55. Ebert MO, Bae SH, Dyson HJ, Wright PE 2008 NMR relaxation study of the complex formed between CBP and the activation domain of the nuclear hormone receptor coactivator ACTR. *Biochemistry* 47:1299–1308
  56. Gao W, Dalton JT, Selective androgen receptor modulator (SARM) binding initiates unique surface topology of androgen receptor AF2 region that alters N/C interaction and co-activator recruitment. 2006 Keystone Symposia, Tissue-Selective Nuclear Receptors, Breckenridge, CO, 2005 (Abstract 207)
  57. Ozers MS, Marks BD, Gowda K, Kupcho KR, Ervin KM, De Rosier T, Qadir N, Eliason HC, Riddle SM, Shekhani MS 2007 The androgen receptor T877A mutant recruits LXXLL and FXXLF peptides differently than wild-type androgen receptor in a time-resolved fluorescence resonance energy transfer assay. *Biochemistry* 46:683–695
  58. Lakowicz JR 2006 Principles of fluorescence spectroscopy. 3rd ed. New York: Springer
  59. Weber G 1992 Protein interactions. New York: Chapman, Hall
  60. Paladini Jr AA, Weber G 1981 Pressure-induced reversible dissociation of enolase. *Biochemistry* 20:2587–2593
  61. Mohana-Borges R, Lima Silva J, de Prat-Gay G 1999 Protein folding in the absence of chemical denaturants. Reversible pressure denaturation of the

- noncovalent complex formed by the association of two protein fragments. *J Biol Chem* 274:7732–7740
62. Mohana-Borges R, Silva JL, Ruiz-Sanz J, de Prat-Gay G 1999 Folding of a pressure-denatured model protein. *Proc Natl Acad Sci USA* 96:7888–7893
63. Desai G, Panick G, Zein M, Winter R, Royer CA 1999 Pressure-jump studies of the folding/unfolding of trp repressor. *J Mol Biol* 288:461–475
64. Phillips JC, Braun R, Wang W, Gumbart J, Tajkhorshid E, Villa E, Chipot C, Skeel RD, Kalé L, Schulten K 2005 Scalable molecular dynamics with NAMD. *J Comput Chem* 26:1781–1802
65. Ponder JW, Case DA 2003 Force fields for protein simulations. *Adv Protein Chem* 66:27–85
66. Wang J, Wolf RM, Caldwell JW, Kollman PA, Case DA 2004 Development and testing of a general amber force field. *J Comput Chem* 25:1157–1174
67. Case DA, Pearlman DA, Caldwell JW, Cheatham TE, Wang J, Ross WS, Simmerling CL, Darden TA, Merz KM, Stanton RV 2002 AMBER7 user manual. San Francisco: University of California, San Francisco
68. DeLano WL 2002 The PyMOL molecular graphics system. San Carlos, CA: DeLano Scientific
69. Humphrey W, Dalke A, Schulten K 1996 VMD: visual molecular dynamics. *J Mol Graph* 14:27–28
70. Kabsch W, Sander C 1983 Dictionary of protein secondary structure: pattern recognition of hydrogen-bonded and geometrical features. *Biopolymers* 22:2577–2637

